Title	A grazing incidence small-angle x-ray scattering analysis on capped Ge nanodots in layer structures.
Author(s)	Okuda, Hiroshi; Kato, Masayuki; Kuno, Keiji; Ochiai, Shojiro; Usami, Noritaka; Nakajima, Kazuo; Sakata, Osami
Citation	Journal of physics: Condensed matter (2010), 22(47)
Issue Date	2010-11-15
URL	http://hdl.handle.net/2433/197168
Right	This is an author-created, un-copyedited version of an article accepted for publication in Journal of Physics: Condensed Matter. The publisher is not responsible for any errors or omissions in this version of the manuscript or any version derived from it. The Version of Record is available online at http://dx.doi.org/10.1088/0953-8984/22/47/474003
Type	Journal Article
Textversion	author

A GISAXS Analysis on Capped Ge Nanodots in Layer Structures

Hiroshi Okuda[1], Masayuki Kato[1], Keiji Kuno[1], Shojiro Ochiai[1], Noritaka Usami[2], Kazuo Nakajima[2], and Osami Sakata[3]

1. Department of Materials Science and Engineering, Kyoto University, Kyoto 606-8501 Japan.

2. Institute for Materials Research, Tohoku University, Katahira, Sendai 980-8577

3. Japan Synchrotron Radiation Research Institute, Spring8 Kohto, Sayo 679-5198 Japan.

Email: okuda@materials.mbox.media.kyoto-u.ac.jp

Abstract. The GISAXS intensity from buried Ge nanodots have been examined both by GISAXS/reflectivity measurements and also simulations with Distorted Wave Born Approximation (DWBA). The validity and the condition of using Born Approximation (BA) are discussed from the simulations based on the layer structures modelled from a reflectivity analysis. As expected in the previous kinematical analysis, use of BA is reasonable in determining the size and the shape of very small or thin nanodots. Several effects of layer structures on the GISAXS analysis have been discussed for further analysis.

1. Introduction

Grazing Incidence Small-Angle X-ray Scattering (GISAXS) has become one of the popular approach to analyze three dimensional nanostructures embedded in or capped under thin layers[1]-[5]. Starting from nanoparticle systems dispersed on polished Si wafer surfaces, GISAXS analysis has been used to examine the nanostructures on a clean surface [4]-[6] and microstructure evolution inside a thin film

deposited on very smooth surfaces[7]-[9]. Concerning nanostructures of self-organizing nanodots, recent developments on in-situ apparatus provide us with real time picture of nanodot growth as reported by Leroy et al.[6] On the other hand, another important question about the microstructure analysis of nanodot is microstructural / interfacial stability of nanodots when they are buried in layers and annealed. For that purpose, structure analysis using Born Approximation (BA) gives straightforward picture. For SAXS analysis in transmission, small changes in the structure parameters such as the gyration radius, the oscillation in the power law region have been examined in cases of phase transformation in metallic alloys.

For GISAXS analysis, however, the corrections on dynamical effect may need to be taken into account. Although it is known that BA is applicable for a large angle of incidence, we still need to know how good the approximation is for a specific condition of GISAXS measurements, to be sure that the change in the structure parameters during annealing, for example, comes from the change in the microstructures, not from the change in the dynamical effect through the change in the reflectivity. In the present report, we made several model calculations under DWBA to discuss the experimental GISAXS patterns.

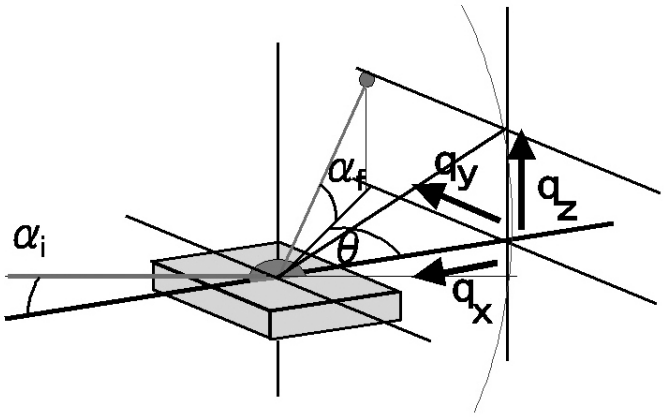

Fig. 1 Schematic illustration of the sample set-up used in the present work. Although the profiles are taken on the Ewald sphere, the profile is approximated to be on the qz-qy plane.

2. Experimental

Figure 1 illustrates the experimental set-up of the present GISAXS experiments. The measurements were made at beam-line 15A of Photon Factory, KEK, Tsukuba Japan. The angle of incidence, α_i, was chosen to be between 0.35 degrees and 0.48 degrees in the present measurements. The detail is described in [3]. Since the GISAXS intensity profiles were measured using two-dimensional detector, the intensity profiles are not exactly on the q_y-q_z plane but on a Ewald sphere with a fixed angle of incidence to be rigorous. This difference becomes important for the samples where the scattering pattern is rather closer to that of diffraction, such as the case for patterned substrates or gratings [10] or when the wave length is large, i.e., the curvature of the Ewald sphere is not negligible, such as the case for GISAXS in the soft X-ray regions[11]. However, in the present case with relatively small

wavelength (0.15 nm) and diffuse scattering, the patterns were well approximated by that on q_y-q_z plane. Specular reflectivity of the sample was measured with a wavelength of 0.100 nm at BL13XU of SPring8, and the layer parameters such as thickness and roughness of the layers were estimated by a least-square fitting of the data for DWBA analysis.

The samples used in the present work were grown by gas-source MBE on a Si (001) substrate and then capped with a Si layer after growing a Ge nanodot layer. The thickness of the Si layer was designed to be about 40 nm. Center part of the substrate was used to avoid spatial heterogeneity in the macroscopic scale.

After evaluating the structure parameters of the nanodots from the GISAXS patterns within a framework of BA[12], DWBA simulations were made with the form factor of nanodot structures obtained from the BA analysis and with layer structures obtained by fitting the specular reflectivity.

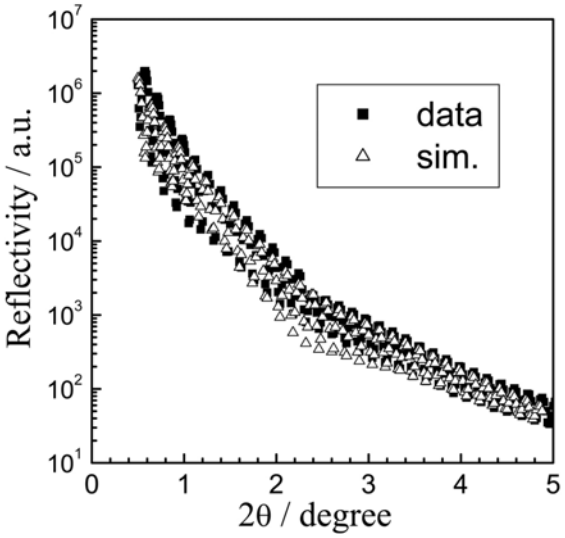

Fig. 2 Specular reflectivity of the sample used for the present GISAXS measurements.

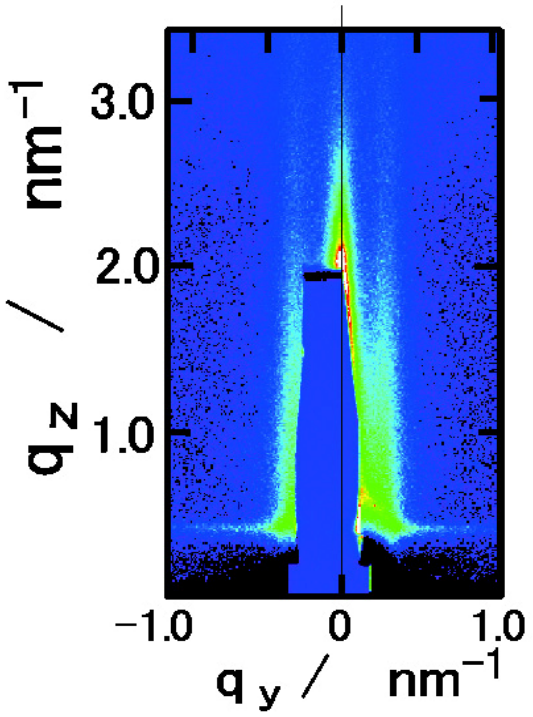

Fig. 3 GISAXS profile of the Ge nanodot sample with a Si cap layer

3. Results and Discussions

Figure 2 gives a specular reflectivity curve of the sample used in the present GISAXS measurements with a fitting result. The layer thickness and roughness parameters were obtained from a least-square fit of the reflectivity, and used to calculate the amplitudes of the wave fields at the nanodot layer in the following DWBA simulations. The thickness of the cap layer was estimated to be 39.5 nm, and the roughness was 0.9 nm for the surface and 0.6 nm nm for the interface. Figure 3 shows a GISAXS pattern of the Ge dot sample measured with an image plate. The in-plane direction of incidence is parallel to [100]. The pattern consists of two principal contributions, namely,

a pair of scattering patterns whose peaks are at q_y=+/- 0.24 nm^{-1}, and a strong streak at q_y=0.0 nm^{-1}. The former corresponds to the SAXS signal from nanodots, and the latter to the diffuse scattering of the interfaces in the layer structures. We shall hereafter call the former as SAXS, and the latter as layer diffuse for simplicity. By using the SAXS pattern outside the interparticle interference peak at q_y=0.24 nm^{-1}, the size and the shape of the buried nanodots were obtained within BA by fitting the intensity at higher q_z to a model form factor having parameters of shape and the size [12].

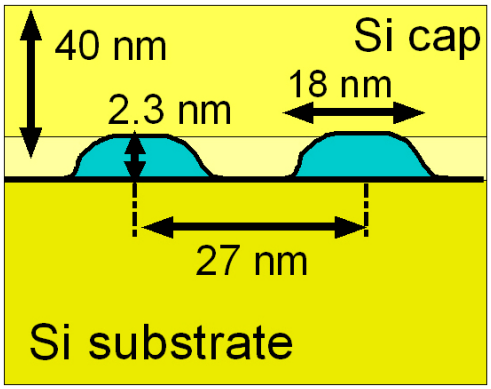

Fig. 4 Size and shape of Ge nanodots obtained from two-dimensional intensity fitting of GISAXS within BA.

Figure 4 illustrates the average sample structure reconstructed from the analysis, with the layer thickness obtained from reflectivity. The average height of the Ge dots is about 2.3 nm, with a base diameter of about 18 nm. The shape, size and interparticle distances obtained from the BA analysis agreed well with the cross-sectional transmission electron microscope images obtained by lattice image[12]. The shape of Ge nanodot, F(r), or its Fourier transform, $\Phi(q)$, was calculated from the analysis, and used for model calculation of GISAXS intensities under BA and DWBA. For the first step of the analysis, an isolated Ge nanodot on a Si substrate and capped with a Si thin layer was assumed.

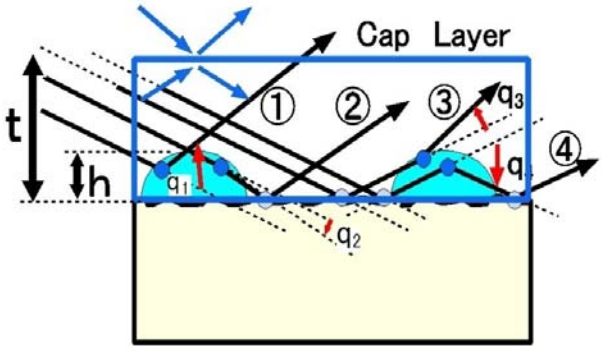

Fig. 5 Schematic illustration of the scattering processes in the present sample.

As shown by Rauscher et al and other researchers [13]-[15], GISAXS intensity from nanodots as depicted in Fig. 4 can be expressed as a sum of four terms. Provided that the shape of the dot is given by F(r), then the total cross section is given by (1) where E(r,k) is the wave field given for the incoming and outgoing ones.

$$A(q,k_i,k_f) = -k_0^2(1-n^2)\frac{e^{ik_0 r}}{4\pi r}\int_v d\vec{r}' E^0(r',-k_f)F(r')E^0(r',k_i) \qquad (1)$$

As schematically shown in Fig.5, the four terms appearing in (1) correspond to the four processes in the figure, as given in the refs. [13]-[16] Since the nanodot layer is placed just on an almost ideally

flat Si substrate, we may first assume that four waves can be treated as in phase. Then the scattering amplitude is written as [15]:

$$A(q,ki,kf) = -k_0^2(1-n^2)\frac{e^{ik_0 r}}{4\pi r}\{T_i T_f \Phi(q_{//}, q_z) + T_i R_f \Phi(q_{//}, -k_z^f - k_z^i) + R_i T_f \Phi(q_{//}, k_z^f + k_z^i) + R^i R^f \Phi(q_{//}, -q_z)\} \quad (2)$$

where Φ(q) is the form factor of the nanodot, and T_i, R_i, T_f and R_f represent the transmission and reflection wave of incoming and outgoing directions, respectively. The amplitudes of the waves at the nanodot layer were calculated by recursive calculations based on Parratt's formula [17] using the layer parameters obtained by fitting specular reflectivity data as mentioned before. To evaluate the effect of corrections by DWBA treatments, the amplitudes of the complex coefficients that cause scattering by nanodot layer were extracted from the DWBA calculation above and shown as a function of total q_z in Fig. 6. The broken lines at q=1.0 nm^{-1} and 1.6 nm^{-1} show the region used to determine the shape and size of nanodot under BA [12]. At the region, the waves that cause corrections by DWBA are more than a couple of order of magnitude smaller than the main term, thereby justifying the shape analysis based on BA. As expected from Fig. 6, the DWBA correction from the T_iR_f term becomes important, with almost the same order of magnitude of the main (Born) term around the Yoneda line. On the other hand, the main contribution at larger q_z comes from the R_iT_f term. The term is more than two orders of magnitude smaller for the present case. The magnitude is mainly determined by the angle of incidence, α_i. Therefore, the correction by the term becomes significant in the cases where very small angle of incidence is required, such as large structures on the surface or polymer films on substrates.

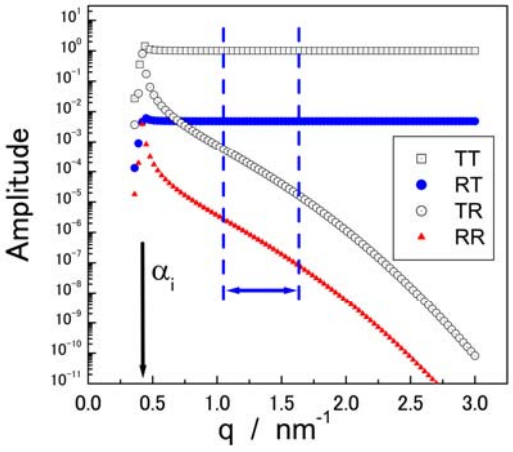

Fig. 6. The coefficients that invokes scattering at the nanodot layer in the present condition. The angle of incidence is shown by an arrow.

In the present DWBA simulation for an isolated nanodot, the squared amplitude of the partial waves were also calculated to examine the contribution to the total scattering intensity.

$$S_i(q) = A_i(q:k_i,k_f)A_i(q:k_i,k_f)^* \quad (3)$$

Figure 7 (a) gives a GISAXS pattern calculated for an isolated and buried Ge nanodot with the size and the shape determined by BA[12]. Oscillations of the calculated intensity were clearly seen owing to that of monodispersed form factor. The lower part of the simulation is shaded by the sample. We have intentionally used rather higher angle of incidence to use BA for convenience of shape and size analysis. Therefore, the total intensity given in Fig. 7 (a) shows just a weak Yoneda line. The

following figures, Fig. 7 (b) to (e) represent the squared partial waves. The figures clearly show that the major part of the total GISAXS intensity is explained by the Born term, where apparent difference from the transmission SAXS is the enhancement of the intensity just on the Yoneda line. As expected from reflectivity curve, the contribution of the other three waves remains very small except near the Yoneda line for the case (d). It is also seen that the oscillation period in the in-plane direction (q_y) appears almost the same for the partial waves. However, as expected from equation (2), this is correct only if the form factor of the nanodot does not depend on q_z, i.e., the shape of the dot is cylindrical or prismatic. When the shape is hemispherical or dome-shaped as for the present case, the composed scattering pattern becomes a sum of intensities from different q_z with the same q_y, having slightly different periodicity as observed in Fig. 7. Conventional analysis such as that for gyration radius may be affected in such a case. For example, in-plane gyration radius may contain systematic error depending on the angle of incidence and also the Fresnel reflectivity when the analysis is made at the region close to the Yoneda line. When one is interested in a quick evaluation of the microstructure from GISAXS pattern, it is useful to know the condition that R_g obtained from GISAXS pattern is a good approximation. Since GISAXS patterns do not contain the region with small q_z, such preliminary analysis is made for line cuts in q_y or q_z direction. Figure 8 (a) and (b) show the Guinier plots of the simulated GISAXS intensity and the components in the cuts in q_y and q_z directions. It is seen that the Guinier plot for the total intensity, S_{total}, shows a good linear relationship with q^2, for the line cut in q_y direction at q_z=0.42 nm^{-1}. Although Fig. 8 (a) represents the cut along the Yoneda line, the slopes agree with each other, and the difference between the slope and those at q_z=0.73 nm^{-1}, where

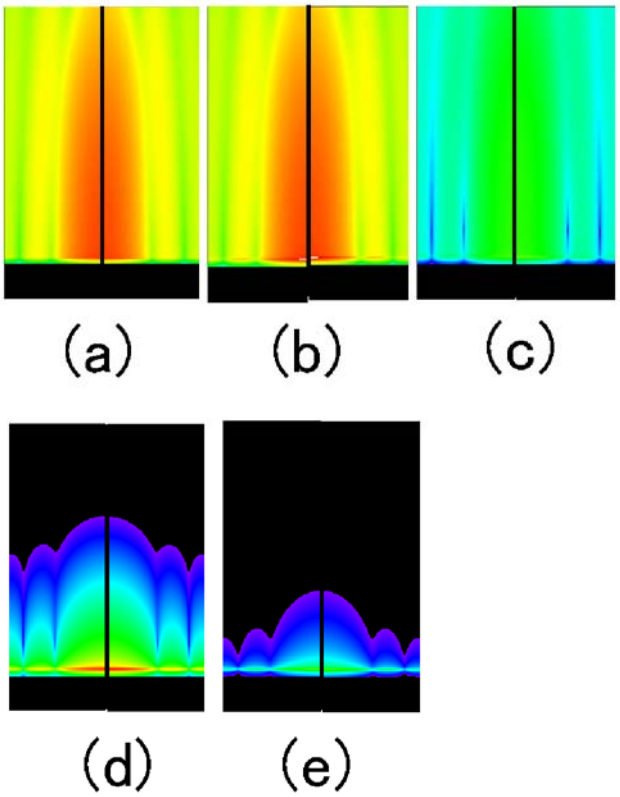

Fig. 7 Calculated total GISAXS intensity (a) and its squared partial waves (b)-(e). The calculation is made for single isolated nanodot having the average size determined by experiments. The figures (b)-(e) correspond to T_iT_f, R_iT_f, T_iR_f, R_iR_f waves drawn with the same scale. The angle of incidence is fixed at 0.48 degree for 0.15 nm of wavelength.

correction by DWBA is expected to be very small, was less than 3%. The difference is explained by the q_z-dependence of the line cuts of the form factor for the present shape of nanodot. Therefore, it is concluded that R_g can be determined better in q_y direction, and even the line cut at the Yoneda line may be a good approximation for the line cuts for kinematical intensity, if the scattering pattern is not smeared by a strong diffuse scattering by the roughness of the surface and interfaces. In contrast, as shown in Fig. 8 (b), the Guinier plots of the total and component intensities look quite different. The deviation from the Guinier plot is explained by the Fresnel coefficients that increase at the Yoneda region for S_{total} and S_1 for the line cuts in q_z direction, not by the effect of correction terms, S_2-S_4, for the present case.

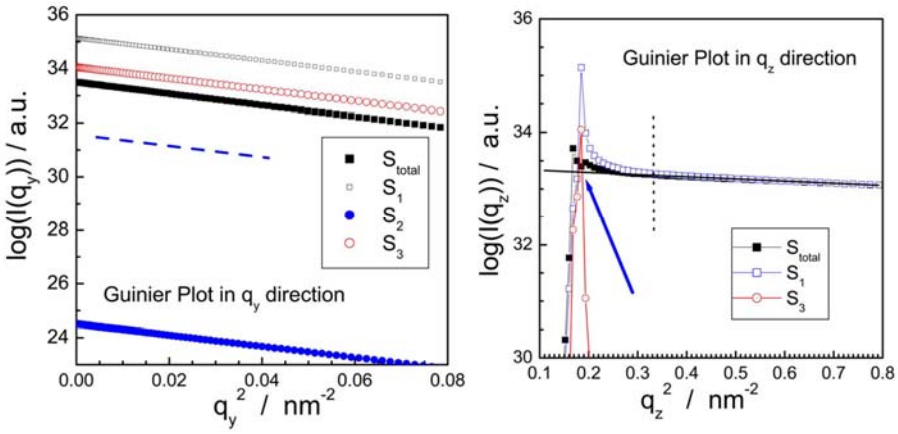

Fig. 8 Guinier plots simulated intensity in q_y and q_z directions. Total intensity and squared partial intensities (S_1-S_3) are plotted. Dynamical effect appears stronger in the line cut along q_z.

In the above discussions, we have used squared amplitudes of the partial waves to discuss the contribution to the total GISAXS intensity. When the contributions of these waves are of the same order of magnitude, then we need to examine how these waves should be summed up. As pointed out by Lee et al., [18], the method might be different depending on the spatial distribution or geometry of scattering objects. In a case of polymer films where the scattering objects distribute with low degree of order inside relatively thick films, the four waves do not necessarily have well-defined phase relationship, and therefore a statistical treatment is required. On the other hand, present sample has a single nanodot layer with a cap layer on top of it. Therefore, the four waves were directly summed for the present case.

Figure 9 gives the argument of the complex amplitude of the waves calculated for the case shown in Fig. 6. Figure 8 (a) corresponds to the phase of total wave, where the four partial waves are summed in complex amplitude. The other four corresponds to the phase of respective partial waves. The trace of inflexion points of the iso-phase line is similar to the shape of the form factor. The shape of the lines for Fig. 8(b) is almost inverted from that of Fig. 8 (e), which can be understood by equation (2). These phase maps suggest that the phase of the total intensity as well as the intensity itself is mostly determined by the first (transmission) term in the present case, but the phase relation of the total intensity might become much more complex when the contribution of other components, in particular,

from those having reverse patterns like (d) and (e) in Fig. 9, is not negligible. In the present simulation for an isolated nanodot, four waves are assumed to be fully coherent, since Ge nanodots in the present sample sit on an atomically flat Si (001) substrate in a single layer. However, the simulated line cut in q_z direction shown in Fig. 8(b) shows a sharp dip at the Yoneda line for S_{total}, although such a dip was not observed in squared partial waves. In the experimental data shown in Fig. 3, no dip was observed. It suggests that two components having principal contribution in the Yoneda region, S1 and S3, give a negative interference owing to the difference in the phase if the waves are fully coherent, which was not observed experimentally. These discrepancies can be explained by assuming that the phases of the transmitted (TT) and reflected-transmitted (RT) waves are not coherent enough to give such a sharp dip in the actual sample, although this result does not affect the conclusion that R_g in the line cut in the q_y direction is regarded as the R_g obtained under the kinematical condition in the present condition. Another effect of incoherence to consider is the effect of the interparticle interference term, where the in-plane distribution of the center of gravity of the nanodots is less regular, which will be discussed later.

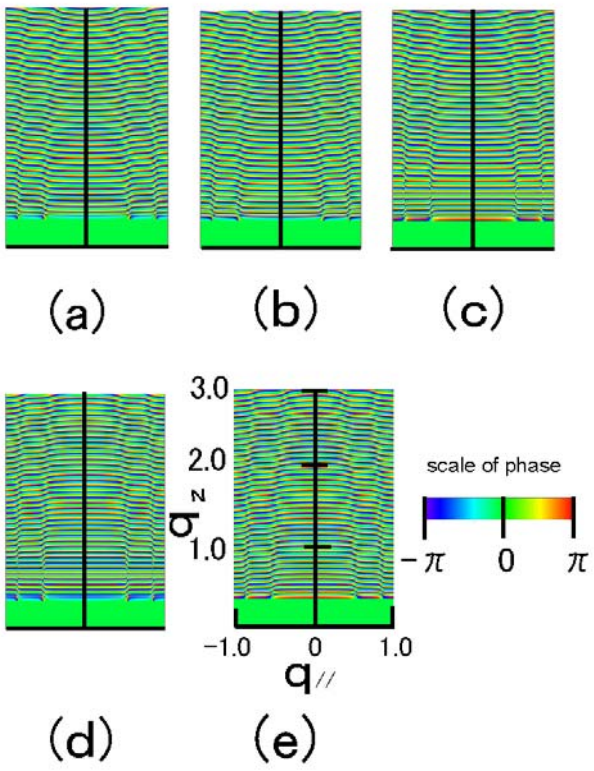

Fig. 9. Arguments calculated for complex amplitude of the total wave (a) and partial waves (b)-(e) corresponding to Fig. 6. The lower part left null is the area where no wave enters. The pattern changes with the sign of the scattering vector defined in eq. (2).

For further analysis on GISAXS intensity, such as how the interface structure of the layers as well as interface between nanodots and cap layer affects the scattering pattern, polydispersity of nanodots have been introduced in the simulation. As shown in Fig. 7, the scattering intensity from monodispersed nanodots shows oscillation which is not observed in experiments. This oscillation is not desirable for detailed analysis, for example, the power law behavior at large q. The SAXS profiles

outside Guinier region, i.e., in the transient region from the Guinier region to the Porod region and also in the Porod region are important when interdiffusion layer of capped nanodot is examined[18]-[20]. Interdiffusion at the dot/cap layer interface during growth and also during post annealing is one of the key factors that affect the properties of the sample. For bulk materials such as semiconducting nanoparticles precipitated in glass matrix, such characterization is made by final slope analysis and also by core-shell analysis [21]-[23]. Final slope analysis is necessary to examine whether the interface is diffuse, and a modified core-shell analysis may be applied to examine the thickness of diffusion layer by examining the transient region from the Guinier to the Porod regime. For GISAXS analysis on the other hand, we need to examine 1. how the power law is affected by the corrections by DWBA, 2. how the layer structures, roughness of the substrate and the cap layer in particular, affect the GISAXS profile. To examine these points, size distribution was introduced in the DWBA simulations to smear out the oscillation of the form factor. We maintained the structure parameters obtained from the simulation the same as the parameters obtained from experiments by adjusting the average radius and the standard deviation of size distribution function. For example, the gyration radii, R_g, is expressed by[23] ;

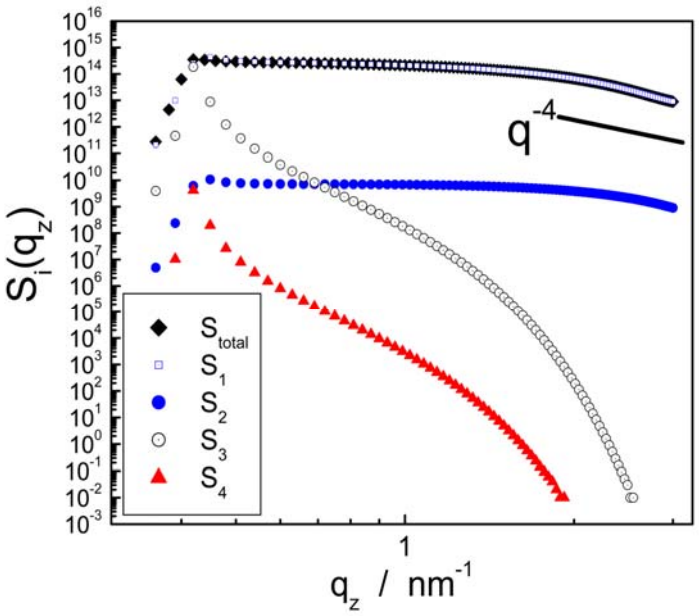

Fig. 10 Simulated intensity profiles along q_z axis. S_{total} is the simulated GISAXS intensity, which almost agrees with the Born term (S_1) except in the Yoneda region.

$$R_g^{\,2} = \int R^8 P(R) dR \Big/ \int R^6 P(R) dR \quad (4)$$

where P(R) is the population of the dot with a radius R. In the present simulation, Gaussian size distribution with the standard deviation of 4 nm is assumed, which is enough to smear out oscillation by the form factor. With the size distribution, GISAXS profile taken at q_y=0.0 in q_z direction is shown in Fig. 10. Total intensity, S_{total} and the four squared partial waves given in (2), S_1-S_4, are plotted as a function of q_z. Figure 10 differs from Fig. 6 in that it reflects the scattering from the nanodots. For simplicity, the interface between the nanodot and the cap layer is assumed to be sharp in the present calculation. The total intensity, S_{total} agreed with the first term, S_1, except the Yoneda region, again confirming that the major part of the GISAXS intensity is explained by the Born (T_iT_f) term.

Comparing S_1 - S_4 in Fig. 10 with four components in Fig. 6, it is concluded that the power law expected for sharp interface in bulk materials is also observed for GISAXS simulation as shown by the slope of q^{-4} in the figure in the region well away from the Yoneda line. However, it is expected that the effect of dynamical correction may not be negligible when the average height of the nanodots becomes more than five times larger than the present size of 2.3 nm, because the Porod region then goes down to the Yoneda line.

The same power law behaviour as in the bulk is explained by the fact that the Born term is the dominant one at large q_z, where power law is observed. The largest correction term in DWBA at large q_z, S_2, has the same q_z dependence as the Born term because the angle of incidence is fixed for the reflection part. Then the effect of correction terms due to reflection can be avoided by taking the incidence angle as large as possible provided that it does not block the low q_z range necessary for the nanostructure analysis included in the layer of interest. Therefore we can conclude that the power law behaviour observed in the q_z direction in GISAXS analysis can be interpreted in the same manner as that for transmission SAXS for bulk materials, as long as only the SAXS signal is measured in the experiment. In contrast, the power law behaviour in the in-plane direction is rather complicated, since the intensity profile in q_y direction at low q_z is strongly affected by the correction term as shown as S_3 in Fig. 10, whose effect is not necessarily negligible depending on the difference in the degree of the decays in the form factor at q_z and (k_i+k_f). A line cut at larger q_z is less affected by the dynamical effect, but the intensity along a constant and large q_z is not a suitable path to examine power law in q_y direction. Therefore, to discuss in-plane power law behaviour from GISAXS profile, use of a DWBA simulation, or at least a two-dimensional BA simulation is necessary.

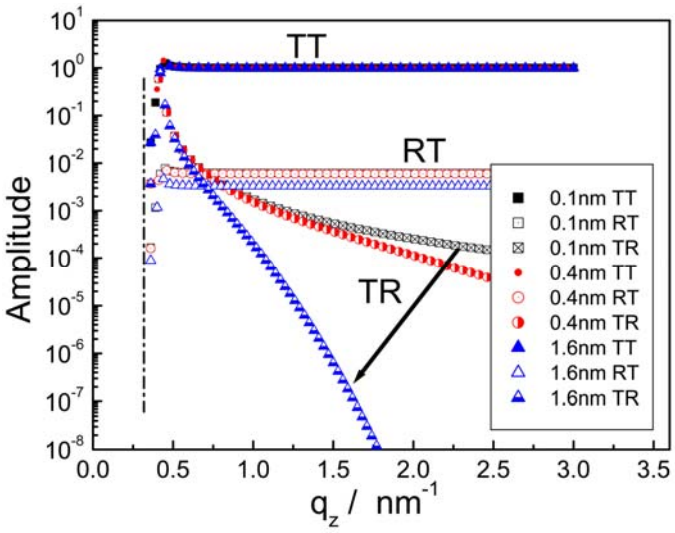

Fig. 11. Effect of surface/interface roughness on the amplitude of three main terms. The roughness applies to all the interfaces. Thickness parameters are the same as those for Fig. 6.

The second point, how the interface roughness affects the evaluation of the GISAXS form factor, can be examined by simulating the magnitude of coefficients for different surface roughness. Figure 11 gives the magnitude of three terms, TT, TR and RT, calculated for ideally smooth surface with a root-mean-square (rms) roughness of 0.1 nm, relatively smooth one with rms roughness =0.4 nm, and rough surfaces with rms roughness of 1.6 nm. It is seen that the main term, TT, is not affected by the

roughness. On the other hand, the RT term which is the major correction term at larger q_z, slightly decreased with roughness. The third term, which is not negligible near the Yoneda wing, shows strong dependence on the roughness as a function of q_z, but the effect remains very small near the Yoneda wing. From these results, it is concluded that the Born term (TT) which gives major contribution at large q_z is not affected by the roughness of the layer structures, and the largest correction terms, i.e., TR term at small q_z and RT term at large q_z, are not strongly affected by the roughness. Therefore, we can conclude that the effect of layer roughness is negligibly small in the final-slope analysis of the GISAXS intensity, and further, if the incident angle is relatively large (a couple of times larger than the critical angle), the power law behavior at large qz in GISAXS is identical to that for bulk transmission SAXS.

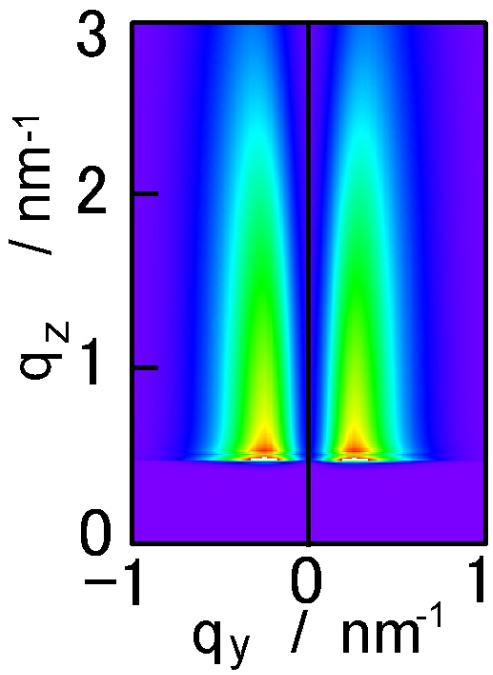

Fig. 12. Effect of surface/interface roughness on the amplitude of three main terms. The roughness applies to all the interfaces. Thickness parameters are the same as those for Fig.7.

Another important point to consider concerning the effect of surface/interface roughness on the GISAXS pattern is that they give diffuse scattering [24] that superimposes GISAXS from nanostructures, as shown in Fig.3 at q_y=0.0. Therefore, large roughness with long correlation length or with roughness correlation between interfaces [25],[26] may alter the GISAXS pattern. To compare the simulated GISAXS intensity with the experiment, interparticle interference was introduced. Figure 12 shows the simulated GISAXS pattern for the experimental one shown in Fig. 3, taking size distribution and interference between nanodots into account. For size distribution, Gaussian distribution is assumed. For the interparticle interference, we adopted local monodisperse approximation (LMA). For bulk materials, the interparticle interference is often treated by LMA [27]. In the present work, the interference effect was also evaluated by LMA in two-dimension. For the present case of single layer nanodot structures, structure function $S(q_y)$ of dot alignment has purely two-dimensional nature. Therefore, the structure function part is not affected by DWBA calculation, which sums up over four different q_z but at the same q_y. Taking the scattering amplitude from a dot with a size R as

$$A(q_{//},q_z) = A_R\{T_iT_f\Phi(q_{//},q_1,R) + R_iT_f\Phi(q_{//},q_2,R) + T_iR_f\Phi(q_{//},q_3,R) + R_iR_f\Phi(q_{//},q_4,R)\} \quad (5)$$

Then the GISAXS intensity is given by,

$$I(q_{//}, q_z) = \int P(R) v^2(R) S(q_{//}, \phi R) A(q_{//}, q_z) A(q_{//}, q_z)^* dR \quad (6)$$

where ϕ is a constant related to the number density of the nanodots and the packing, and $\nu(R)$ is the volume of a nanodot having size R. Comparing the simulated pattern and the experimental one shown in Fig.3, they agree : 1.The shape, peak position in q_y (interparticle distance) and in-plane and out-of-plane radius of gyration. 2. Position of Yoneda line. On the other hand, however, the intensity profiles along q_z at q_y=0 nm^{-1} do not agree. Clear intensity minimum is observed for the simulation due to the structure function was observed in Fig. 12, while strong diffuse scattering was observed in the experimental profile. Fortunately, the diffuse scattering from surface/interface roughness scattering and GISAXS from nanodot structure appeared in the almost separate regions of the scattering profile in the present sample. This is the most important reason that we could discuss GISAXS profile without direct simulation of diffuse scattering from layer interface in the present sample.

From DWBA simulation of the nanodot modelled from BA analysis of GISAXS measurements of capped Ge nanodots, the validity of using BA in the shape and size analysis of buried nanodot samples and its conditions have been confirmed.

4. Conclusions

With a use of DWBA simulation, analysis of GISAXS profiles from Ge nanodot capped with a thin Si layer has been discussed from a viewpoint that how far the BA is applicable, and also how the layer structure of the sample may affect the GISAXS pattern. DWBA simulation with size distribution and local monodisperse approximation provided simulated patterns that agreed with the measured two-dimensional GISAXS intensities except interfacial diffuse scattering. It is concluded that the shape of the nanodots and the power law behavior at large q_z can be analyzed by simple Born approximation when the angle of incidence is reasonably large, and under some conditions as discussed here, a Guinier analysis even along the Yoneda line is an acceptable aproximation.

References

[1] A. Naudon *Modern Aspects of Small-angle scattering*, ed. H.Brumberger,1990 Kluwer p181.

[2] J.Stangl, V.Holy and G.Bauer *Rev. Mod. Phys.* **76** (2004)725.

[3] H.Okuda et al, *Appl. Phys. Lett.*, 81(2002)2358.

[4] R. Paniago, H. Metzger, M Rauscher.et al., *J.Appl. Cryst*., **33** (2000) 433.

[5] G. Renaud ,R.Lazzari, C.Revenant, et al., *Science* **300** (2003) 1416.

[6] F. Leroy et al., *J.Cryst. Growth* **275**(2005)e2195.

[7] P.Müller-Buschbaum et al., *Spectrochem. Acta,* B**59** (2004). 1789.

[8] S.Jin, J. Yoon, K. Heo et al., *J. Appl. Crystl.*, **40**(2007)950.

[9] H. Yokoyama, C.Dutriez, L.Li et al., *J. Chem. Phys.* **127**(2007)014904.
[10] M. Yang and A. Gibaud, *J. Appl. Cryst.*, **40**(2007) 1050.
[11] H. Okuda, M. Kato, S. Ochiai and Y. Kitajima, *Appl. Phys. Express* **2**(2009)126501.
[12] T. Ogawa, H.Niwa, H.Okuda et al. *Mater. Sci. Forum* 475-479(2005)1097.
[13] M. Rauscher, R. Paniago, H. Metzger et al., *J.Appl. Phys*. **86**(1999) 6763.
[14] R. Lazzarri *J. Appl. Cryst*. **35**(2002) 406.
[15] M.Rauscher *Phys. Rev.* **B52**(1995)16855.
[16] B. Lee, J. Yoon, W. Oh et al., Macromolecules **38**(2005)3395.
[17] L.G. Parratt *Phys. Rev.* **95**(1954)359.
[18] B.-D. Lee , J. Yoon, W. Oh et al., *Macromolecules* **38**(2005),3395.
[19] G. Porod, *Kolloid Z.* **24**(1951)93.
[20] P.W.Schmidt *J. Appl. Cryst*., **24**(1991)414.
[21] Small-angle X-ray Scattering, ed. O. Kratky and O. Glatter, Academic Press,N.Y.1983.
[22] L.A. Feigin and D. Svergun Structure Analysis by Small-Angle X-ray and Neutron Scattering, Plenum, N.Y. 1987.
[23] R. Bauer and V.Gerold *Acta Metall*., **12**(1964)1449.
[24] S.K. Sinha, E.B. Sirota, S. Garoff nd H.B. Stanley, *Phys. Rev.* **B38**(1988) 2297.
[25] V.Holy and T.Baumbach *Phys. Rev*. **B49**(1994)10688.
[26] J.P. Schlomka, M.Tolan, L.Schwalowsky et al., *Phys. Rev*. **B51**(1995)2311.
[27] J.S. Pedersen, *Phys. Rev.* **B47** (1993) 657.